Estimating Average Dielectric Properties for Microwave Breast Imaging Using Focal Quality Metrics

Declan O'Loughlin, Finn Krewer, Martin Glavin, Edward Jones, Martin O'Halloran

***Abstract*—Confocal Microwave Imaging algorithms synthetically focus backscattered radar signals to create an image of the breast. Spatial focusing is achieved by delaying the received signals by the round-trip propagation delay to the voxels of interest. A key component in calculating propagation time is a good estimate of the average dielectric properties of the breast, because the accuracy of the reconstructed image varies significantly with the value of average dielectric properties used.**

This paper investigates the use of focal quality metrics to estimate the optimal average dielectric properties to use to reconstruct an image of the breast. Focal quality metrics have long been used to find optimally focused images in microscopy and camera systems without prior knowledge of the imaged object's location or texture. In this paper, five common focusing algorithms from autofocus and shape-from-focus applications are compared to investigate whether these focal quality metrics can be used to estimate the patient-specific average dielectric properties.

***Index Terms*—focal quality metrics, microwave imaging, breast cancer detection, autofocus techniques, biomedical imaging**

I. Introduction

Microwave imaging exploits dielectric contrasts between cancerous and healthy tissues at microwave frequencies to detect breast tumours. Confocal Microwave Imaging (CMI) is one widely used method to convert the microwave reflections into useful images of the breast [1]–[8]. CMI beamformers synthetically focus backscattered signals from each voxel in the imaging area successively to construct an energy profile of the breast. Regions of high energy in the resultant images suggest the presence of a significant dielectric scatterer (i.e. a tumour). This image reconstruction technique is based on a number of assumptions [9], primarily:

- that sufficient contrast in dielectric properties exists between healthy tissues and tumours;
- that the dielectric properties of the breast are such that coherent addition can occur at scatterers;
- and that representative average dielectric properties can be found which can be used to estimate propagation delays and synthetically focus signals.

Many different methods have been used to estimate the average dielectric properties to ensure a clear and focused image of the breast can be formed. Originally, published dielectric properties of adipose tissues were used [1], [2], [5], [6], [8], [10]. Others considered the skin and immersion medium, but still used published values of dielectric properties of adipose tissues for the breast interior [3], [7]. However, there is often a considerable difference between these published values and the patient-specific average dielectric properties. This difference in estimated average dielectric properties results in an incorrect estimation of the average microwave propagation speed, and therefore a poorly reconstructed CMI breast image. Improved performance was demonstrated in [11] where the average dielectric properties of the interior of the breast were calculated from the backscattered signals using inverse scattering. Time-of-flight measurements were used to estimate interior properties in numerical studies [12], while promising multi-path propagation measurements were used in some experimental studies [13], [14].

Rather than adding an additional step to the microwave breast imaging procedure to estimate the microwave propagation speed, the authors propose the use of focal quality metrics (FQMs) to optimise the assumed average dielectric properties. The FQMs presented in this paper are analysed to see if image quality is correlated with a well-focused image. If good correlation is established, then there is potential to use the FQM as a method to fine-tune the average dielectric estimate, and consequently to optimise the microwave breast image.

The remainder of the paper is structured as follows: Section II describes the FQMs used and the rational for their selection; Section III describes how the chosen FQMs are evaluated in terms of fitness and the images on which they are analysed; Section IV describes the results and Section V concludes the paper.

II. Focal quality Metrics

In this paper, five FQMs were described and compared. FQMs can broadly be divided based on their method of action, and one metric from each of the families identified in a recent review of FQMs were chosen in this paper [15]. In general, FQMs operate by estimating the high-frequency spatial content of the image [16].

A. Gradient-based focal quality metric (Φ_G)

Approximations to the first derivative or gradient of the image have been widely used as FQMs, [15], [17]–[22]. The first-order difference of the image is commonly used as a computationally efficient estimation of the first spatial derivative, and is used in this work. The absolute value of the gradient is analysed here, which is commonly used as a

metric. All dimensions are considered, the maximum of the absolute gradient along each direction is used.

$$\Phi_{\mathrm{G}} = \frac{1}{XY} \sum_x \sum_y \max_{D \in \{X,Y\}} |I_D(x,y)| \tag{1}$$

where X and Y are the dimensions of the image and I_X and I_Y are the first-order differences along the X and Y dimensions respectively.

B. Laplacian-based focal quality metrics (Φ_L)

Similar to Φ_{G}, Laplacian-based methods use second-order differentiation to reward high-frequency content in the image. The energy of the Laplacian is a commonly used FQM [15], [16], [23], [24] and is defined as:

$$\Phi_{\mathrm{L}} = \frac{1}{XY} \sum_x \sum_y (L * I) \tag{2}$$

where L is the discrete approximation to the Laplacian given by:

$$L = \frac{1}{6} \begin{pmatrix} 1 & 4 & 1 \\ 4 & -20 & 4 \\ 1 & 4 & 1 \end{pmatrix} \tag{3}$$

C. Wavelet-based focal quality metric (Φ_W)

Statistics of the high-frequency sub-bands of the discrete wavelet transform (DWT) have also been used as FQMs [15], [25]–[27]. In this work, the absolute sum of the three detail sub-bands calculated with a first-level DWT and a db6 filter (Daubechies filter with six vanishing moments) was used:

$$\Phi_{\mathrm{W}} = \frac{1}{XY} \sum_x \sum_y |I_{LH}(x,y)| + |I_{HL}(x,y)| + |I_{HH}(x,y)| \tag{4}$$

where I_{LH}, I_{HL} and I_{HH} are the first-level detail sub-bands.

D. Fourier-based focal quality metric (Φ_F)

Statistics of the coefficients of the Discrete Cosine Transform (DCT) have been investigated as FQMs [15], [28]–[30]. The ratio of the AC energy to the DC energy is used:

$$\Phi_{\mathrm{F}} = \frac{1}{XY} \sum_x \sum_y \frac{\sum_{(n,m) \neq (0,0)} F_{x,y}(u,v)^2}{F_{x,y}(0,0)^2} \tag{5}$$

where $F_{x,y}$ is the DCT of the $N \times M$ sub-block centered at (x,y). $M = N = 8$ is used in this work.

E. Statistics-based focal quality metric (Φ_S)

Various statistics of the grey-level luminance of the image have also been used as FQMs. In this paper, a commonly used statistic — the variance of the grey-level luminance — is analysed [15], [17]–[20], [22], [31]:

$$\Phi_{\mathrm{S}} = \frac{1}{XY} \sum_x \sum_y (I(x,y) - \bar{I})^2 \tag{6}$$

where $\bar{I}$ is the mean of the image.

III. Evaluation of focal quality metrics

This section describes how FQMs are traditionally evaluated, and how these qualities can be analysed in the context of CMI.

A. Characteristics of an effective focal quality metric

This section describes some commonly identified characteristics currently used to evaluate FQMs in other applications and identifies similar characteristics important in CMI. Three important characteristics are:

- independence from image content; [20], [32]
- the extremum is located at the correct value (accuracy); [19], [22], [32].
- monotonic with respect to blur [20].

In the context of CMI, independence from the contents of the image is measured by repeating the results for a number of tumour locations. Accuracy is measured by estimating the parameters using the FQM and comparing this to the parameters of the best-case image generated using *a priori* knowledge of the average dielectric properties of the breast. Monotonicity is measured by correlating the FQM using Spearman's rank correlation coefficient, ρ, against an estimation of the similarity of the images to the best-case image, a similarity curve. The similarity curve is generated by comparing each image to the image generated using the best-case average dielectric properties. SSIM is used to compute the similarity of the images [33].

B. Experimental Evaluation

This section describes the models used in Finite-Difference Time-Domain simulations of the breast used to evaluate the FQMs. A homogenous breast with a realistic skin layer is considered when evaluating the performance of the FQMs. The in-breast relative permittivity value and that of the matching medium in which the breast is immersed were chosen to be similar to adipose tissues, $\varepsilon_r = 3.74$. The skin layer has a relative permittivity of, $\varepsilon_r = 35.14$, and the tumour has a relative permittivity of, $\varepsilon_r = 60.33$. Twenty different models were created, each with a spherical tumour of radius between $3\,\mathrm{mm}$ and $5\,\mathrm{mm}$ randomly placed within the breast.

The breast phantom is illuminated with a single-cycle sine wave modulated by a Gaussian pulse. The excitation pulse has a centre frequency of $6\,\mathrm{GHz}$ and a bandwidth of $6\,\mathrm{GHz}$. Twenty equally spaced antennas arranged in a cylindrical configuration successively illuminate the breast and monostatic signals are recorded. Ideal skin subtraction is used to isolate the tumour response. Although unrealistic, ideal skin subtraction algorithm is used because the paper is solely focused on image sharpness and focus.

A monostatic Delay-and-Sum beamformer is used to generate the images [9] with a window length equal to the width of the pulse in the time-domain. Two hundred and one images were generated for each model, using an average value of relative permittivity varying from between 3 to 23 in steps of 0.1.

TABLE I
ACCURACY AND CORRELATION TO THE SIMILARITY CURVE RESULTS. RANKING INDICATED IN PARENTHESES (LOWER IS BETTER). BEST-CASE AVERAGE RELATIVE PERMITTIVITY, $\varepsilon_r = 5.2$.

Metric	Accuracy		Correlation (ρ)	
	μ	σ	μ	σ
Φ_{L}	5.01 (4)	0.38	-0.83 (4)	0.15
Φ_{G}	5.05 (3)	0.27	-0.93 (1)	0.07
Φ_{S}	5.30 (2)	0.66	-0.89 (2)	0.10
Φ_{W}	5.20 (1)	0.49	-0.88 (3)	0.14
Φ_{D}	3.03 (5)	0.09	-0.32 (5)	0.31

IV. RESULTS

This section details the results of evaluating the FQMs listed in Section II by the method explained in Section III.

The results are structured as follows:

- Figure 1 compares the images generated with different average relative permittivities along with a cross-section of the breast model;
- Figure 1a shows the breast coronal cross-section at the tumour location;
- Figures 1b to 1h show the images generated with average relative permittivities, $\varepsilon_r = 3, 4, \ldots, 9$ respectively.

A. Quantative evaluation

Table I shows the accuracy and monotonicity with respect to blur of each of the five FQMs. For each criterion, the average, μ, and the standard deviation, σ, across the twenty models is calculated. The FQMs are then ranked by each criterion. The best-case average relative permittivity is 5.2. Φ_{L}, Φ_{S}, Φ_{G} and Φ_{W} all accurately predict the best average relative permittivity to within $\Delta\varepsilon_r = 0.2$. On average, Φ_{W} is the most accurate. Φ_{G} has the highest value of ρ, with the smallest standard deviation. Φ_{D} fails to accurately predict the relative permittivity, and also shows poor values of ρ. Φ_{D} estimates a value of 3 each time which is the lowest of the range of permittivities analysed.

B. Focal Quality Metric curves

Figure 2 shows the FQM curves for the five FQMs. Also shown is the similarity curve as described in III-A. The best-case image is chosen by calculating the exact average dielectric properties of the imaging area. Visually, Φ_{L}, Φ_{S}, Φ_{G} and Φ_{W} all correctly identify the correct speed to use which is indicated by an SSIM of 1 (identical to the best-case image). Φ_{G}, Φ_{W} and Φ_{S} are equally sharp at the extremum, that is, the width of the peaks is similar. In contrast, Φ_{L} exhibits a considerably broader peak. However, any accurate FQM can be artifically sharpened by raising it to a power [17]. This means that a broad peak is not a good criterion on which to judge an FQM. Φ_{D} does not correctly identify the average relative permittivity. Although some peaks are exhibited in the correct locations, the value of the metric at the start of the curve (the lowest average relative permittivity), is greater than at any of the subsequent peaks.

V. CONCLUSIONS

These results show that FQMs could potentially be used to estimate the dielectric properties of a breast used when generating a CMI image. This is necessary for realistic screening scenarios when estimating the average dielectric properties of the breast in advance could be difficult. FQMs could be used to adaptively estimate the average dielectric properties and generate an image of higher quality.

Further work will focus on choosing the best FQM for CMI applications, testing the FQMs in more complex heterogenous scenarios, and expanding the two-dimensional FQMs used in shape-from-focus and auto-focus applications to three-dimensional volumes.

ACKNOWLEDGMENT

This work was supported by the Irish Research Council (Grant no. RCS1326), Science Foundation Ireland (Grant no. 12/IP/1523 and 1l/SIRG/I2120) and the MiMED COST Action (TD1301).

REFERENCES

[1] E. C. Fear and M. A. Stuchly, "Confocal microwave imaging for breast tumor detection: a study of resolution and detection ability," in *Engineering in Medicine and Biology Society, 2001. Proceedings of the 23rd Annual International Conference of the IEEE*, vol. 3. IEEE, 2001, pp. 2355–2358.

[2] R. Nilavalan, A. Gbedemah, I. J. Craddock, X. Li, and S. C. Hagness, "Numerical investigation of breast tumour detection using multi-static radar," *Electron. Lett.*, vol. 39, no. 25, pp. 1787–1789, 2003.

[3] Hooi Been Lim, Nguyen Thi Tuyet Nhung, Er-Ping Li, and Nguyen Duc Thang, "Confocal Microwave Imaging for Breast Cancer Detection: Delay-Multiply-and-Sum Image Reconstruction Algorithm," *IEEE Trans. Biomed. Eng.*, vol. 55, no. 6, pp. 1697–1704, Jun. 2008.

[4] M. Klemm, I. J. Craddock, J. A. Leendertz, A. Preece, and R. Benjamin, "Improved Delay-and-Sum Beamforming Algorithm for Breast Cancer Detection," *Int. J. Antennas Propag.*, vol. 2008, pp. 1–9, 2008.

[5] D. Byrne, M. O'Halloran, M. Glavin, and E. Jones, "Data independent radar beamforming algorithms for breast cancer detection," *Prog. Electromagn. Res.*, vol. 107, pp. 331–348, 2010.

[6] M. O'Halloran, E. Jones, and M. Glavin, "Quasi-Multistatic MIST Beamforming for the Early Detection of Breast Cancer," *IEEE Trans. Biomed. Eng.*, vol. 57, no. 4, pp. 830–840, Apr. 2010.

[7] E. C. Fear, J. Bourqui, C. Curtis, D. Mew, B. Docktor, and C. Romano, "Microwave Breast Imaging With a Monostatic Radar-Based System: A Study of Application to Patients," *IEEE Trans. Microw. Theory Tech.*, vol. 61, no. 5, pp. 2119–2128, May 2013.

[8] A. Shahzad, M. O'Halloran, E. Jones, and M. Glavin, "A preprocessing filter for multistatic microwave breast imaging for enhanced tumour detection," *Prog. Electromagn. Res. B*, vol. 57, pp. 115–126, 2014.

[9] S. C. Hagness, A. Taflove, and J. E. Bridges, "Two-dimensional FDTD analysis of a pulsed microwave confocal system for breast cancer detection: Fixed-focus and antenna-array sensors," *Biomed. Eng. IEEE Trans. On*, vol. 45, no. 12, pp. 1470–1479, 1998.

[10] D. Byrne and I. J. Craddock, "Time-Domain Wideband Adaptive Beamforming for Radar Breast Imaging," *IEEE Trans. Antennas Propag.*, vol. 63, no. 4, pp. 1725–1735, Apr. 2015.

[11] D. Winters, E. Bond, B. Van Veen, and S. Hagness, "Estimation of the Frequency-Dependent Average Dielectric Properties of Breast Tissue Using a Time-Domain Inverse Scattering Technique," *IEEE Trans. Antennas Propag.*, vol. 54, no. 11, pp. 3517–3528, Nov. 2006.

[12] M. Sarafianou, I. J. Craddock, T. Henriksson, M. Klemm, D. Gibbins, A. Preece, J. Leendertz, and R. Benjamin, "MUSIC processing for permittivity estimation in a Delay-and-Sum imaging system," in *7th European Conference on Antennas and Propagation (EuCAP)*, 2013, pp. 839–842.

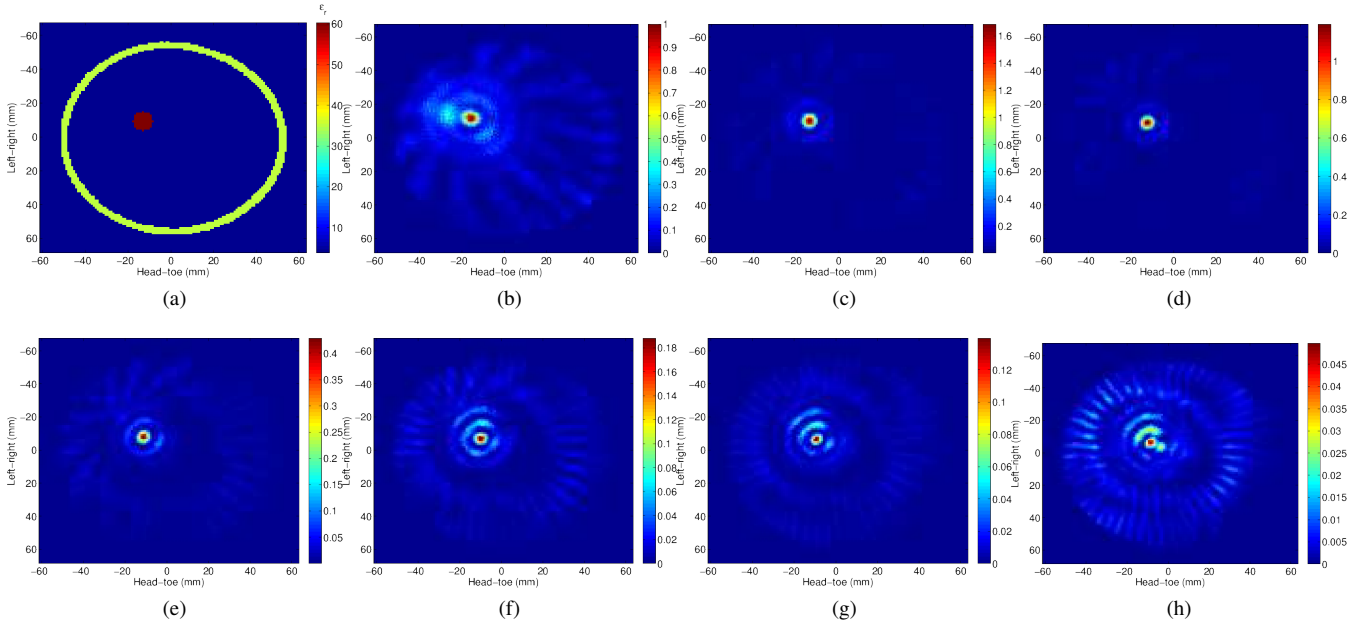

Fig. 1. (a) shows a two-dimensional cross-section of the breast model. (b) – (h) show images reconstructed with permittivities, $\varepsilon_r = 3, 4, \ldots, 9$ respectively. (d) shows the best localization and least noise as it closest to the best average relative permittivity, while other images are successively poorer.

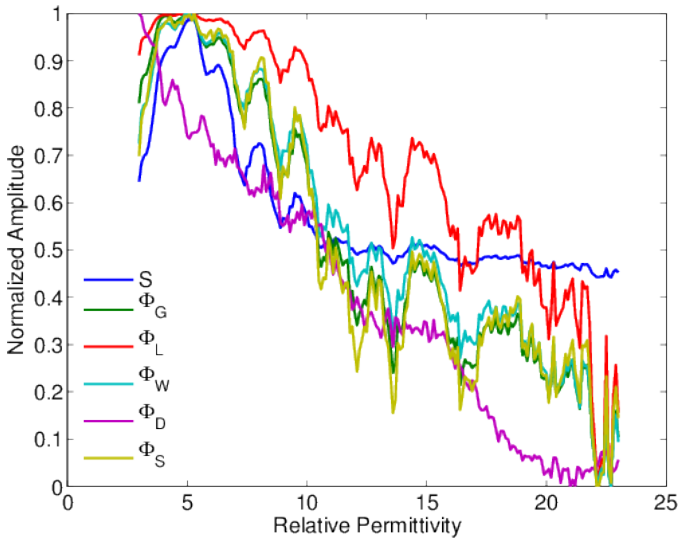

Fig. 2. This figure comparing the FQM curves. For the given model (cross-section as shown in Figure 1a), the normalized value of each FQM is shown. For comparison, the similarity curve is also shown. This is calculated by comparing each image to the best-case image using SSIM. The best-case image is chosen by using the exact average relative permittivity of the imaging volume. All but Φ_D follow the same trend as the SSIM.

[13] J. D. Garrett and E. C. Fear, "Average property estimation validation with realistic breast models," in *Antennas and Propagation (EuCAP), 2014 8th European Conference on*. IEEE, 2014, pp. 1279–1280.

[14] J. Garrett and E. Fear, "Average Dielectric Property Analysis of Complex Breast Tissue with Microwave Transmission Measurements," *Sensors*, vol. 15, no. 1, pp. 1199–1216, Jan. 2015.

[15] S. Pertuz, D. Puig, and M. A. Garcia, "Analysis of focus measure operators for shape-from-focus," *Pattern Recognit.*, vol. 46, no. 5, pp. 1415–1432, May 2013.

[16] J. F. Schlag, A. C. Sanderson, C. P. Neuman, and F. C. Wimberly, "Implementation of Automatic Focusing Algorithms for a Computer Vision System with Camera Control." DTIC Document, Tech. Rep., 1983.

[17] M. Subbarao, T.-S. Choi, and A. Nikzad, "Focusing techniques," *Opt. Eng.*, vol. 32, no. 11, pp. 2824–2836, 1993.

[18] A. SANTOS, C. ORTIZ DE SOLÓRZANO, J. J. VAQUERO, J. M. PEÑA, N. MALPICA, and F. DEL POZO, "Evaluation of autofocus functions in molecular cytogenetic analysis," *J. Microsc.*, vol. 188, no. 3, pp. 264–272, 1997.

[19] Y. Sun, S. Duthaler, and B. J. Nelson, "Autofocusing in computer microscopy: Selecting the optimal focus algorithm," *Microsc. Res. Tech.*, vol. 65, no. 3, pp. 139–149, Oct. 2004.

[20] W. Huang and Z. Jing, "Evaluation of focus measures in multi-focus image fusion," *Pattern Recognit. Lett.*, vol. 28, no. 4, pp. 493–500, Mar. 2007.

[21] J. F. Brenner, B. S. Dew, J. B. Horton, T. King, P. W. Neurath, and W. D. Selles, "An automated microscope for cytologic research a preliminary evaluation." *J. Histochem. Cytochem.*, vol. 24, no. 1, pp. 100–111, 1976.

[22] L. Firestone, K. Cook, K. Culp, N. Talsania, and K. Preston, "Comparison of Autofocus Methods for Automated Microscopy," *Cytometry*, vol. 12, no. 3, pp. 195–206, 1990.

[23] R. A. Muller and A. Buffington, "Real-time correction of atmospherically degraded telescope images through image sharpening," *JOSA*, vol. 64, no. 9, pp. 1200–1210, 1974.

[24] A. Erteza, "Sharpness index and its application to focus control," *Appl. Opt.*, vol. 15, no. 4, pp. 877–881, 1976.

[25] G. Yang and B. J. Nelson, "Wavelet-based autofocusing and unsupervised segmentation of microscopic images," in *Intelligent Robots and Systems, 2003.(IROS 2003). Proceedings. 2003 IEEE/RSJ International Conference on*, vol. 3. IEEE, 2003, pp. 2143–2148.

[26] J.-T. Huang, C.-H. Shen, S.-M. Phoong, and H. Chen, "Robust measure of image focus in the wavelet domain," in *Intelligent Signal Processing and Communication Systems, 2005. ISPACS 2005. Proceedings of 2005 International Symposium on*. IEEE, 2005, pp. 157–160.

[27] H. Xie, W. Rong, and L. Sun, "Wavelet-based focus measure and 3-d surface reconstruction method for microscopy images," in *Intelligent Robots and Systems, 2006 IEEE/RSJ International Conference on*. IEEE, 2006, pp. 229–234.

[28] J. Baïna and J. Dublet, "Automatic focus and iris control for video cameras," in *Image Processing and its Applications, 1995., Fifth International Conference on*. IET, 1995, pp. 232–235.

[29] C.-H. Shen and H. H. Chen, "Robust focus measure for low-contrast images," in *Consumer Electronics, 2006. ICCE'06. 2006 Digest of Technical Papers. International Conference on*. IEEE, 2006, pp. 69–70.

[30] S.-Y. Lee, J.-T. Yoo, Y. Kumar, and S.-W. Kim, "Reduced Energy-Ratio Measure for Robust Autofocusing in Digital Camera," *IEEE Signal Process. Lett.*, vol. 16, no. 2, pp. 133–136, Feb. 2009.

[31] N. N. K. Chern, P. A. Neow, and M. H. Ang Jr, "Practical issues in pixel-based autofocusing for machine vision," in *Robotics and Automation, 2001. Proceedings 2001 ICRA. IEEE International Conference on*, vol. 3. IEEE, 2001, pp. 2791–2796.

[32] F. C. Groen, I. T. Young, and G. Ligthart, "A Comparison of Different Focus Functions for Use in Autofocus Algorithms," *Cytometry*, no. 6, pp. 81–91, 1985.

[33] Z. Wang, A. Bovik, H. Sheikh, and E. Simoncelli, "Image Quality Assessment: From Error Visibility to Structural Similarity," *IEEE Trans. Image Process.*, vol. 13, no. 4, pp. 600–612, Apr. 2004.